

# The Parkin co-regulated gene product, PACRG, is an evolutionarily conserved axonemal protein that functions in outer-doublet microtubule morphogenesis

Helen R. Dawe\*, Helen Farr\*, Neil Portman, Michael K. Shaw and Keith Gull†

Sir William Dunn School of Pathology, University of Oxford, South Parks Road, Oxford, OX1 3RE, UK

\*These authors contributed equally to this work

†Author for correspondence (e-mail: keith.gull@path.ox.ac.uk)

Accepted 23 August 2005

Journal of Cell Science 118, 5421-5430 Published by The Company of Biologists 2005

doi:10.1242/jcs.02659

## Summary

Eukaryotic cilia and flagella are highly conserved structures composed of a canonical 9+2 microtubule axoneme. Comparative genomics of flagellated and non-flagellated eukaryotes provides one way to identify new putative flagellar proteins. We identified the Parkin co-regulated gene, or *PACRG*, from such a screen. Male mice deficient in *PACRG* are sterile, but its function has been little explored. The flagellated protozoan parasite *Trypanosoma brucei* possesses two homologues of *PACRG*. We performed RNA interference knockdown experiments of the two genes independently and both together. Simultaneous ablation of both proteins produced slow growth and paralysis of the flagellum with consequent effects on organelle segregation. Moreover, using transmission electron microscopy, structural defects were seen in the axoneme, with microtubule doublets missing

from the canonical 9+2 formation. The occurrence of missing doublets increased toward the distal end of the flagellum and sequential loss of doublets was observed along individual axonemes. GFP fusion proteins of both *PACRG* homologues localised along the full length of the axoneme. Our results provide the first evidence for *PACRG* function within the axoneme, where we suggest that *PACRG* acts to maintain functional stability of the axonemal outer doublets of both motile and sensory cilia and flagella.

Supplementary material available online at  
<http://jcs.biologists.org/cgi/content/full/118/23/5421/DC1>

Key words: Pacrg, Axoneme, Outer-doublet microtubule, Outer-doublet linkages

## Introduction

Cilia and flagella are highly conserved structures that are found on a wide range of cell types and expressed in many different organisms. Cilia and flagella are adapted to perform a large number of functions (El Zein et al., 2003) from motility to mechanosensation. They are typically composed of a microtubule axoneme made up of nine outer-doublet microtubules. In addition to this, motile cilia and flagella usually contain inner- and outer-dynein arms on these doublet microtubules and a central pair of two singlet microtubules.

Comparative bioinformatics demonstrates conservation between known flagellar proteins. Comparison of the genomes of flagellated organisms with those of non-flagellated organisms such as plants, red algae and yeast (e.g. *Arabidopsis thaliana*, *Cyanidioschyzon merolae* and *Schizosaccharomyces pombe*) allows for the identification of novel putative flagellar proteins. We analysed the published human ciliary proteome (Ostrowski et al., 2002) for evolutionarily conserved proteins of unknown function. One of these, annotated only as a hypothetical in the original publication, was revealed by our bioinformatics analyses to be *PACRG*, a protein that was identified subsequent to the proteomic investigation.

*PACRG* was originally identified (West et al., 2003) as a gene lying upstream of, and sharing a common promoter with *Parkin*, the gene implicated in juvenile Parkinson's disease. The quaking mouse (Sidman et al., 1964) is a spontaneous mutation with a large deletion in chromosome 17 that results in the loss of expression of both *Parkin* and *PACRG* (Lockhart et al., 2004). Mice have tremors characteristic of Parkinson's disease and in addition, male homozygotes are sterile. *PACRG* loss has been recently identified as the cause of the male sterility component of this phenotype (Lorenzetti et al., 2004). However, its function remains unknown. We hypothesised that *PACRG* might play a role in the flagellum. This idea is supported by two further analyses using a comparative bioinformatics approach to search for putative flagellar proteins (Avidor-Reiss et al., 2004; Li et al., 2004), in which *PACRG* is found.

The protozoan parasite *Trypanosoma brucei* is an excellent model organism in which to study cilia and flagella because of its well-characterised cytoskeleton (for a review, see Gull, 1999) and its genetic tractability. It possesses a single flagellum, which exits at the posterior end of the cell from the flagellar pocket and is attached to the cell body along its length,

proceeding to the anterior tip of the cell. As well as the axoneme, the flagellum contains an additional structure, the paraflagellar rod (PFR). This lattice-like structure runs alongside the axoneme, to which it is attached. At cell division, the cell maintains the old flagellum and assembles a new flagellum.

Here we show that *T. brucei* contains two PACRG paralogues. Using RNA interference (RNAi) in *T. brucei* to address the function of PACRG, we show that simultaneous knockdown of both paralogues produces paralysed flagella. At the ultrastructural level we observe loss of specific outer-doublet microtubules. We show that occurrence of missing outer doublets increases along the length of the flagellum. GFP-PACRG fusion proteins localise along the full length of the axoneme. We propose that PACRG performs a novel function within eukaryotic flagella in maintaining interdoubtlet linkages and thus preserves axoneme integrity.

## Materials and Methods

### Bioinformatics

Sequences for TbPACRG A and TbPACRG B were obtained from GeneDB (<http://www.genedb.org/>) and used to perform BLAST searches (Altschul et al., 1997) on publicly available databases (<http://genome.jgi-psf.org/chlre2/chlre2.info.links.html> and <http://www.ncbi.nlm.nih.gov/BLAST/>). Homologues were identified by reciprocal BLAST searches and alignments created using ClustalX (Thompson et al., 1997).

### Constructs and trypanosome transfection

For individual TbPACRG A or TbPACRG B RNAi, 600 bp fragments of the relevant gene were amplified by PCR with TbPACRG A or B specific primers (TbPACRG A forward, ATGAGTTACGAGATAC; TbPACRG A reverse, CGTTGCGCAAAT; TbPACRG B forward, ATGGCGTTCTCACGAA; TbPACRG B reverse, GACGTTA-ATGAT) incorporating *Xba*I and *Hind*III restriction sites into the forward and reverse primers, respectively. For TbPACRG AB RNAi, the same 600 bp fragment of each gene was amplified using the same primer sequences. For TbPACRG A an *Xba*I site was added to the forward primer and *Eco*RI to the reverse primer; for TbPACRG B, an *Eco*RI site was added to the forward primer and *Hind*III to the reverse primer. Fragments were cloned into the p2T7-177-inducible RNAi vector (Wickstead et al., 2002) using the *Xba*I and *Hind*III sites. Procyclic *T. brucei* 29-13 cells (Wirtz et al., 1999) were transfected using standard protocols, selected using 5 µg/ml phleomycin, and subsequently cloned by limiting dilution.

To make cell lines expressing endogenously tagged GFP-TbPACRG fusion protein, 150-200 bp fragments of the 5' end of each TbPACRG gene, and within the 5' untranslated region (UTR) were amplified with TbPACRG A or B specific primers incorporating suitable restriction sites and ligated into a vector for GFP expression (S. Kelly and K.G., unpublished). Trypanosomes were transfected, and selected using 50 µg/ml hygromycin.

### Culture of trypanosomes

Cell lines were cultured in SDM 79 medium supplemented with 10% foetal calf serum and appropriate antibiotics at 28°C. For RNAi, cells were induced using 1 µg/ml doxycycline.

### Analysis of motility

Non-induced cells and induced cells after 72 hours were grown to a density of  $2 \times 10^6$  cells/ml. The motility of these cells was analysed as described by (Gadelha et al., 2005). Cells were tracked for 20 frames,

taken over 40 seconds. Movie 1 in supplementary material shows the normal motility of the trypanosome flagellum and the phenotype of cells 72 hours after induction in tissue culture flasks. Cells were examined using a Zeiss Axiovert 35M inverted microscope with a  $32 \times$  lens and video was captured using a COHU High Performance CCD camera onto a DMR-E85H DVD video recorder (Panasonic).

### Immunolocalisation studies and antibodies

For DNA staining, cells were settled onto glass slides, fixed in 3.6% formaldehyde (TAAB) in phosphate-buffered saline (PBS) and embedded in Vectashield (Vector Laboratories) with 4,6-diamidino-2-phenylindole (DAPI). For co-immunofluorescence, trypanosomes were settled onto glass slides, cytoskeletons prepared by extraction with 1% NP-40 in 100 mM PIPES, pH 6.9, 2 mM EGTA, 1 mM MgSO<sub>4</sub>, 0.1 mM EDTA and fixed in 1.8% formaldehyde in PBS for 10 minutes. Cells were double-labelled with anti-GFP (rabbit polyclonal A11122, Invitrogen) and either anti-PFR (L8C4) (Kohl et al., 1999) or anti-basal body (BBA4) (Woods et al., 1989). Secondary antibodies were Alexa-488-conjugated anti-rabbit (A-11034, Molecular Probes) and Alexa-546-conjugated anti-mouse (A-11030, Molecular Probes). Cells were embedded in Vectashield with DAPI. Slides were examined on a Zeiss Axioplan 2 microscope using a  $100 \times$ , 1.4 NA oil-immersion lens, captured on a CCD camera controlled by Metamorph software (Universal Imaging) and processed in Metamorph and Adobe Photoshop (Adobe).

### Preparation of cells for thin-section TEM

Cells were fixed at 72 hours after induction of RNAi in 2.5% glutaraldehyde, 2% paraformaldehyde and 0.1% picric acid in 100 mM phosphate (pH 6.5) for 2 hours at 4°C followed by post-fixation in 1% osmium tetroxide in 100 mM phosphate buffer (pH 6.5) for 1 hour at 4°C. The fixed material was stained en bloc with 2% aqueous uranyl acetate for 2 hours at 4°C. Following dehydration through a graded series of acetone and propylene oxide, the material was embedded in epon resin for sectioning and analysis by transmission electron microscopy.

### Statistical analysis

Chi-squared and Student's *t*-tests were carried out using Excel (Microsoft).

### Real-time quantitative PCR

Total RNA samples were collected from the 29-13 parental cell line, non-induced cells and induced cells 24 hours and 48 hours after induction. RNA samples were purified using silica gel-based purification methods (High Pure RNA Isolation Kit, Roche) and stored at  $-80^\circ\text{C}$ . Synthesis of cDNA from 1 µg RNA was carried out using the Omniscript Reverse Transcription Kit (Qiagen), with oligo(dT) primers at a final concentration of 1 µM. Three reverse transcription reactions were carried out from each RNA sample. Single stranded cDNA products were then analysed by Q-PCR using TaqMan probes against PACRG A, PACRG B and QM, a 60S ribosomal protein used as a reference gene. A no RT control was used to measure DNA contamination. For each gene, primers were designed using Oligo4 (DNASar) to amplify a 100-130 bp region. (PACRG A forward, GATGTCGGCGATTGGTTAT; PACRG A reverse, TCTCATACGTCGGCACCATA; PACRG B forward, AAATACACGACACCCAACCTG; PACRG B reverse, GTAGAGATT-GAACACCGGAA; QM forward, GCGTGCCAACAAGGAATGT; QM reverse, GCGAAGTACGTGGAACGGA). Products were detected using TaqMan probes (PACRG A, TCATGGTGGCG-ACGATGCGT; PACRG B, AACTTGTGGAGAGCGCCGAC; QM, CCACATGCGTATCCGCGCCC) with 6-FAM on the 5' end and BHQ-1 on the 3' end. Concentrations of primers, probes and MgCl<sub>2</sub>

for each primer set were optimised prior to the experiment. In each PCR cycle the fluorescence was recorded at the end of the annealing phase. The *Ct* value for each reaction was measured, and the absolute DNA amount calculated. For each sample this was normalised against the reference gene, QM, and then expressed as a percentage of the level in 29-13 cells.

**Results**

**Two PACRG family members in *Trypanosoma brucei***

To determine the genome occurrence pattern of PACRG, we interrogated publicly available databases with the mouse Pacrg protein sequence. PACRG homologues were found to be widely conserved among flagellated organisms, including *Caenorhabditis elegans* (Fig. 1). Sequences showed most homology in the C-terminal region as shown by the large blocks of dark blue indicating identical residues in Fig. 1. Homologues were not found in the genomes of non-flagellated organisms including *Arabidopsis thaliana*, *Cyanidioschyzon merolae* and *Schizosaccharomyces pombe*. In the protozoan parasite *T. brucei*, we found two paralogues with a high degree of conservation. These are equally divergent from mouse Pacrg, and therefore we named them TbPACRG A and TbPACRG B. TbPACRG A and B are conserved within the kinetoplastids *Leishmania major* and *Trypanosoma cruzi* in addition to *T. brucei*.

**Ablation of both TbPACRG mRNAs produces slow growth and paralysis**

To understand the function of PACRG in *T. brucei*, we used RNAi to ablate protein expression of the two PACRG family members both independently and together. Ablation of TbPACRG A or TbPACRG B alone produced no effect on cell growth rate (Fig. 2B,D respectively) or cell division (data not shown), although the RNA levels fell to 9% (Fig. 2A) and 8% (Fig. 2C) of the parental (29-13 cell line) level respectively. A no-RT control showed minimal DNA contamination. However, simultaneous ablation of TbPACRG A and B, with a reduction of TbPACRG A to 10% and TbPACRG B to 20% (Fig. 2E), produced a slow growth phenotype first apparent at 72 hours post-induction (Fig. 2F). Induced cells appeared morphologically normal by phase-contrast microscopy (Fig. 3, compare A,B to C,D), however in 27% cells undergoing cytokinesis (*n*=200) we observed incorrect positioning of the kinetoplast (Fig. 3). In some cells the kinetoplast was closer than normal to the nucleus (Fig. 3, compare distance between nucleus and kinetoplast in A to that in E), whereas in others it was positioned almost anterior to the most posterior daughter nucleus (Fig. 3F, arrow indicates posterior kinetoplast). In each case of mispositioning, the kinetoplast that is most affected tends to be that associated with the new flagellum, located at the posterior end of the cell. We also observed a small increase in the number

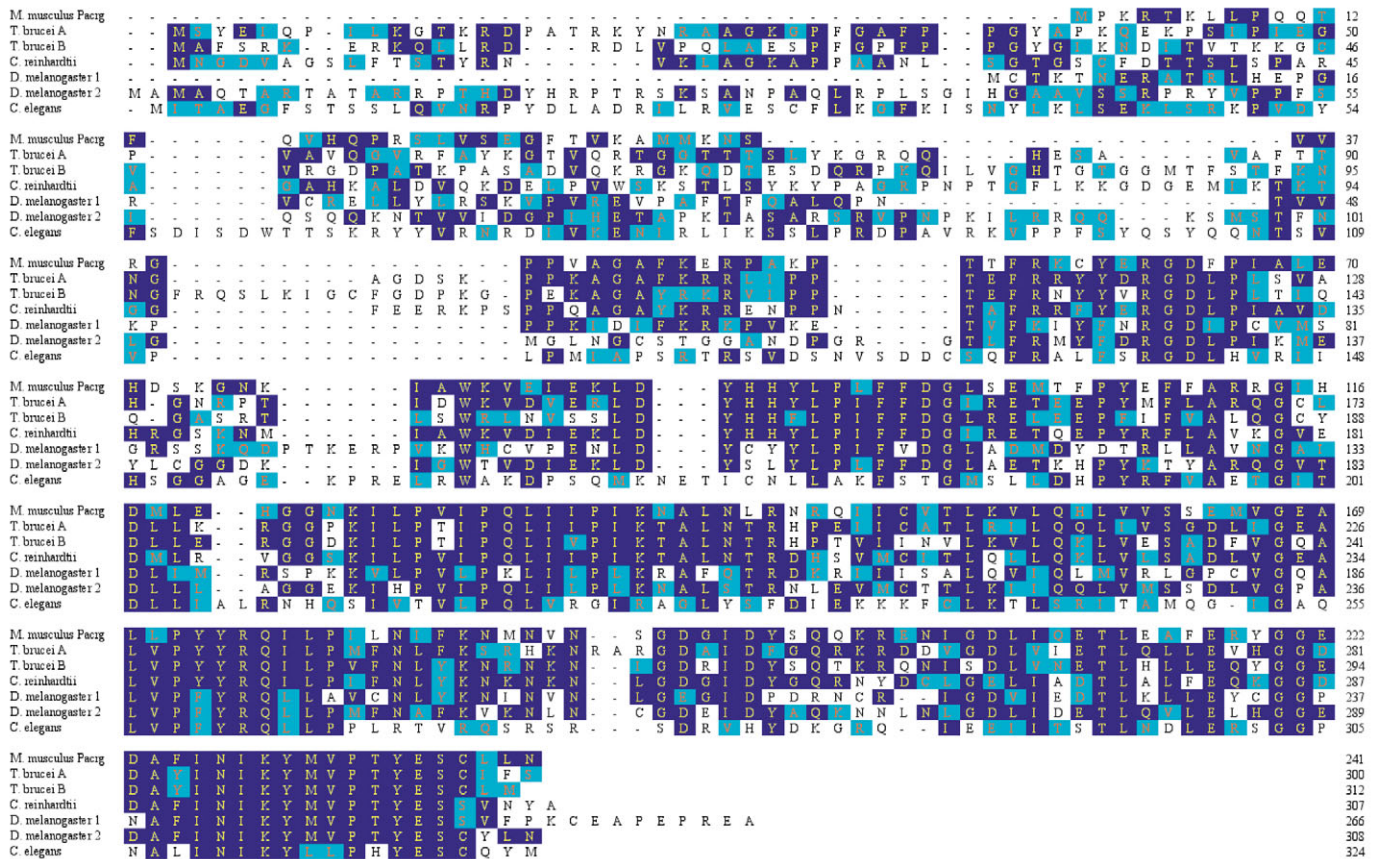
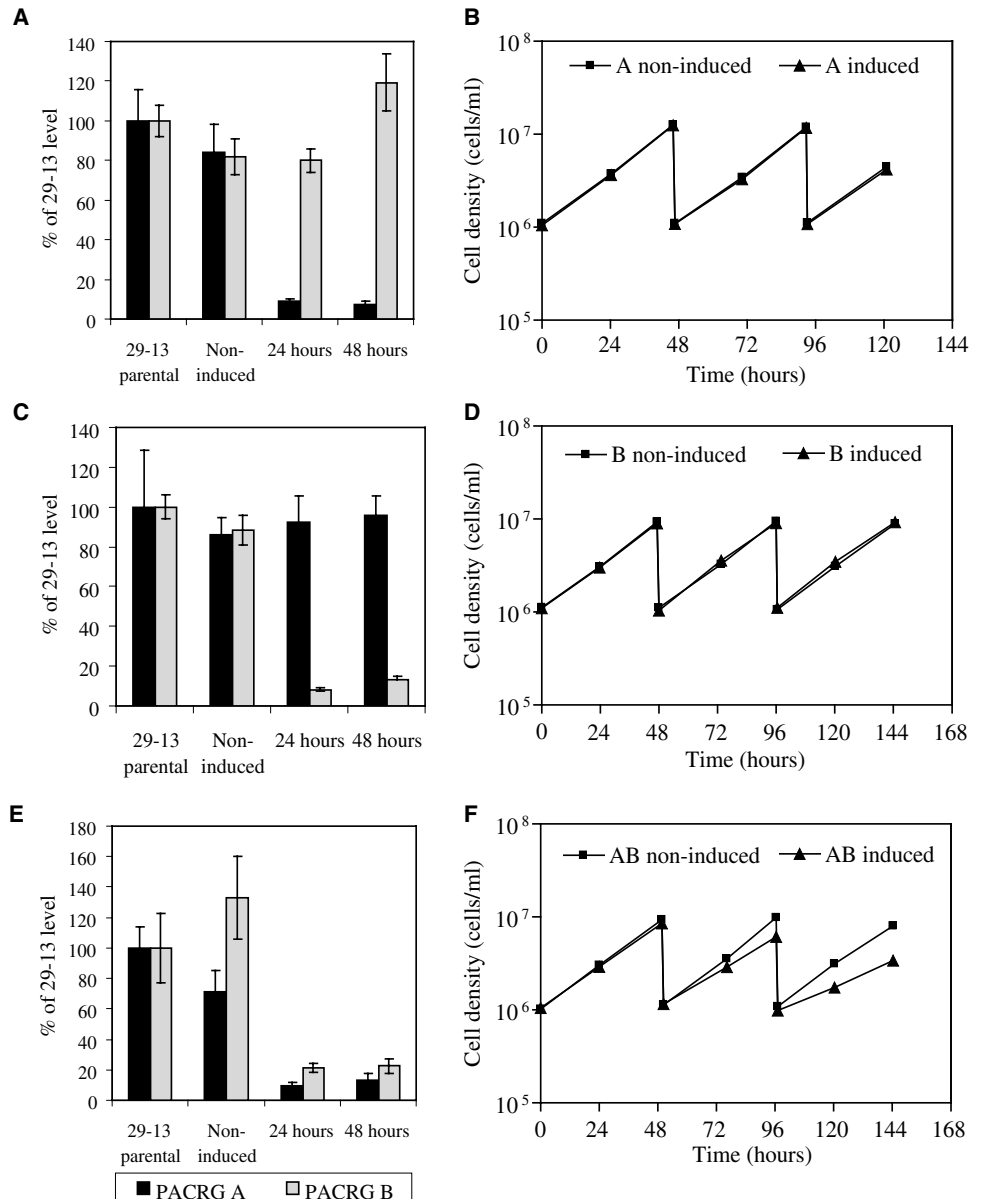


**Fig. 1.** Two PACRG paralogues in *T. brucei*. Protein sequence alignment of two *T. brucei* PACRG-like proteins (Tb03.4808.210 and Tb09.210.1470) with gene products from *M. musculus* (XP\_128418), *C. reinhardtii* (C\_20334), *D. melanogaster* (CG179349 and CG15120) and *C. elegans* (NP\_495496). Orthology was determined by examination of candidate sequences including reciprocal BLAST. Identical residues are shown in dark blue; similar residues are shown in light blue.

**Fig. 2.** Ablation of PACRG AB produces a slow-growth phenotype. Q-PCR data (A,C,E) and representative growth curves (B,D,F) of cells undergoing RNAi of TbPACRG A (A,B), TbPACRG B (C,D) or TbPACRG AB (E,F). A reduction of mRNA signal of TbPACRG A (black bars) was seen in RNAi TbPACRG A-treated cells (A). However, there was no alteration in growth kinetics in TbPACRG A RNAi-treated cells (B, triangles) compared to non-induced controls (B, squares). A reduction of mRNA signal of TbPACRG B (grey bars) was observed in RNAi TbPACRG B-induced cells (C), but again, no alteration in growth kinetics was observed compared to the control (D). A reduction of mRNA signal of TbPACRG A (black bars) and TbPACRG B (grey bars) was observed in TbPACRG AB RNAi-treated cells (E) with the representative growth curve (F) showing a growth defect starting 72 hours after induction (triangles) compared to non-induced controls (squares). For the growth curves (B,D,F), cells were maintained in log phase by diluting the culture every 48 hours. Q-PCR values are percentages (mean $\pm$ s.e.m.) of the control cell signal (A,C,E).



of cells with two nuclei and two kinetoplasts (17% of the population in PACRG AB RNAi-induced cells compared to 12% in non-induced controls), suggesting that RNAi-induced cells have difficulties in late phases of the cell cycle.

We observed that TbPACRG AB RNAi-induced cells possessed flagella of normal length (20.3 $\pm$ 0.6  $\mu\text{m}$  in non-induced cells;  $n=100$ , compared with 20.3 $\pm$ 0.6  $\mu\text{m}$  in induced cells;  $n=100$ ) and continued to build a new flagellum each cell cycle. However, cell motility was strongly affected. At 24 hours after induction, 20% of cells had a paralysed flagellum ( $n=108$  cells) and did not move. By 48 hours, this had increased to 48% ( $n=102$  cells), and at 72 hours after induction, 73% of flagella ( $n=48$  cells) were paralysed (see also supplementary material Movie 1, compare the induced cells to the non-induced cells). By tracking locomotion of a cohort of individual cells in the population over the course of 40 seconds we were able to measure their speed. Highly significant differences ( $P<0.001$ ) were observed between RNAi-induced

( $n=53$ ) and non-induced cells ( $n=38$ ) in terms of minimum, mean and maximum speeds (Table 1).

#### TbPACRG AB RNAi induction causes loss of outer-doublet microtubules

To understand the paralysis of the flagellum, we prepared TbPACRG AB RNAi-induced and non-induced cells for

**Table 1. Induction of TbPACRG AB RNAi causes a severe loss in motility**

Population motility parameter	Non-induced (n=38)	Induced (n=53)
Minimum speed ( $\mu\text{m}/\text{second}$ )	1.1 $\pm$ 0.2	0.1 $\pm$ 0.1
Mean speed ( $\mu\text{m}/\text{second}$ )	3.0 $\pm$ 0.2	0.8 $\pm$ 0.1
Maximum speed ( $\mu\text{m}/\text{second}$ )	4.8 $\pm$ 0.3	1.6 $\pm$ 0.2

Speeds shown are the average minimum, mean and maximum speeds for a population of TbPACRG AB RNAi-induced and non-induced cells.

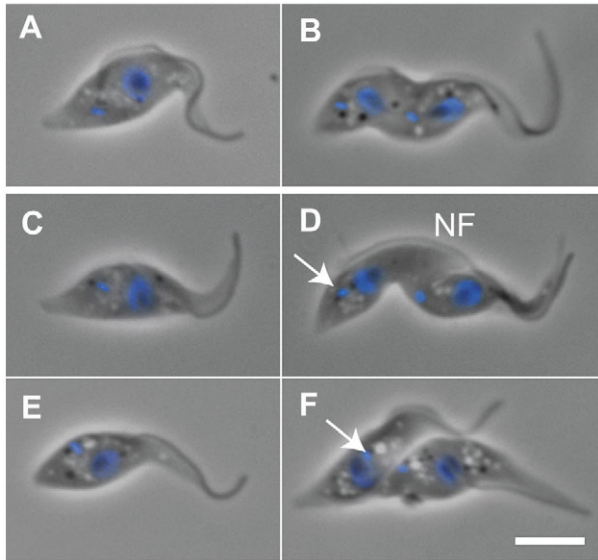


**Fig. 3.** Induced cells build a flagellum, however daughter kinetoplast position is impaired. Phase-contrast images of control cells (A,B) and TbPACRG AB RNAi-induced cells at 72 hours (C-F) with nuclear and kinetoplast DNA overlaid in blue. (A) A non-induced cell with one kinetoplast and one nucleus (1K1N). (B) A non-induced cell with duplicated nucleus and kinetoplast (2K2N cell) showing correct positioning of both kinetoplasts. (C) A TbPACRG AB RNAi-induced cell with correct positioning of the kinetoplast. (D) A TbPACRG AB RNAi-induced cell undergoing division where the distance between the daughter kinetoplast (arrow) and the daughter nucleus is reduced compared to that of the parent cell. Note the formation of the new flagellum (NF). (E) A TbPACRG AB RNAi-induced 1K1N cell where the kinetoplast is mislocated. (F) A TbPACRG AB RNAi-induced cell undergoing cytokinesis where the daughter kinetoplast (arrow) is mispositioned, anterior to the daughter nucleus. Bar, 5  $\mu$ m.

ultrastructural analysis by thin-section transmission electron microscopy. We observed a significant difference in the 9+2 architecture of the trypanosome flagellum. In non-induced control cell profiles, 98% ( $n=922$ ) possessed a canonical 9+2 axonemal arrangement (Fig. 4A, a). In contrast, 53% ( $n=953$ ,  $P<0.001$ ) of axonemal profiles in induced TbPACRG AB RNAi cells exhibited loss of at least one of the nine outer-doublet microtubules (Fig. 4A, b-d). A minority of flagella profiles in TbPACRG AB RNAi-induced cells (4%) contained

one or more displaced doublets outside the partial axoneme (data not shown). The number of missing doublets varied; approximately equal numbers of 8+2, 7+2, 6+2 and 5+2 axonemes were observed. The central pair microtubules generally remained present until more than four outer-doublet microtubules had been lost (Fig. 4A, b and c). Axonemes containing four or fewer outer-doublet microtubules lacked the central pair in 88% of cases (Fig. 4Ad). We observed cells that were in division ( $n=50$ ) and had two adjacent flagella profiles (the old flagellum and the newly built flagellum). At cell division the cell maintains the old flagellum and assembles a new flagellum; late in the cell cycle it is possible to distinguish between the two (Sherwin and Gull, 1989). Of the cell profiles

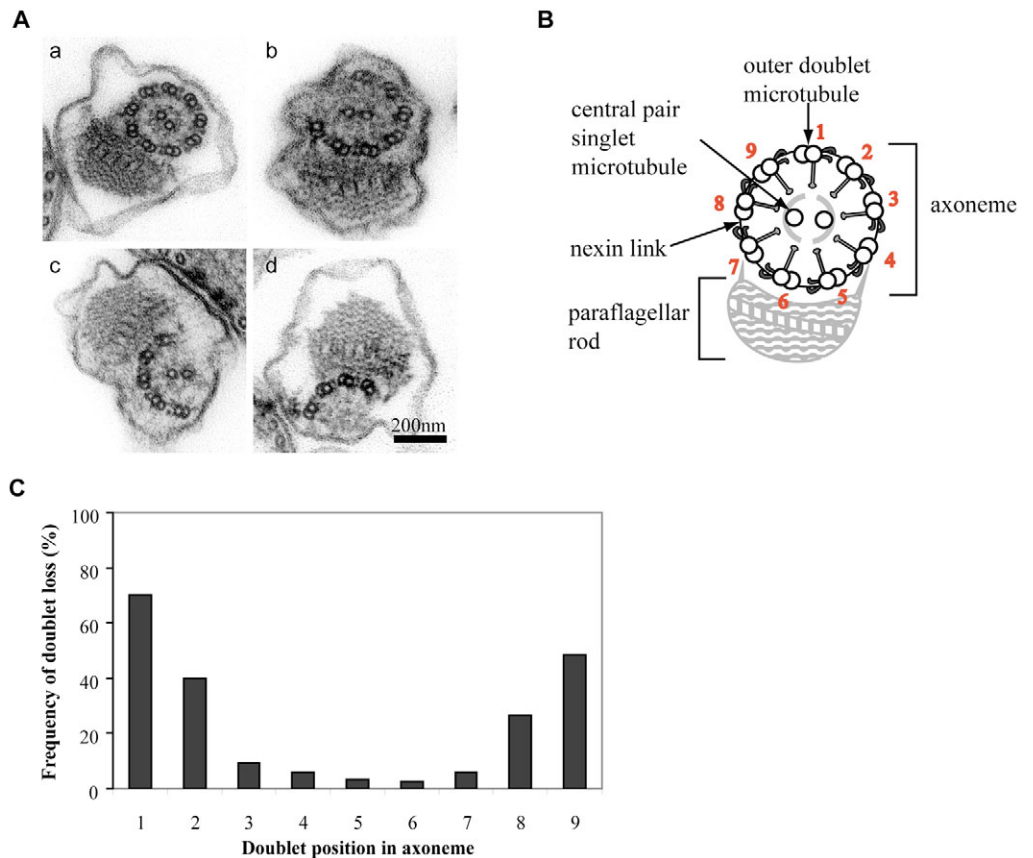


**Fig. 4.** PACRG AB RNAi induction causes loss of outer-doublet microtubules. (A) Transmission electron microscopy images of TbPACRG AB non-induced cells (a) and RNAi-induced cells 72 hours after induction (b-d). Note the loss of variable numbers of outer-doublet microtubules in b-d. (B) Drawing of relevant structures in a *T. brucei* flagellum. Numbers refer to the convention of numbering outer doublets according to their position relative to the central pair and PFR. (C) Graph of frequency of loss of specific outer-doublet microtubules. Bar, 200 nm.

examined, 51% had two affected flagella, with at least one outer doublet missing from each; 18% of cell profiles exhibited one unaffected old flagellum and one affected new flagellum; the remainder had two unaffected flagella.

We investigated whether particular outer-doublet microtubules were more susceptible to loss. In *T. brucei*, outer doublets are numbered according to their position relative to the central pair and the PFR (Fig. 4B), with the doublet directly opposed to the central pair being numbered as 1 and stable connections to the PFR on doublets 4 and 7. Where multiple doublets had been lost, it was nearly always adjacent doublets that were absent (see Fig. 4Ab for an example). We found that the doublets furthest from the PFR, doublets 9 and 1, were most likely to be lost, followed by doublets 2 and 8 (Fig. 4C). The doublets adjacent to the PFR were rarely missing; doublets 4 and 7, which are most obviously attached to the PFR (Fig. 4B) were missing in only 4.7% of axonemes, whereas doublets 5

and 6 were absent in only 2.6% and 2.1% of axonemes, respectively (Fig. 4C).

#### Outer-doublet microtubule number decreases towards the distal tip of the flagellum

Variability in the number of missing doublets raised the possibility that there could be a variation in the number of missing doublets along the length of an individual axoneme in TbPACRG AB RNAi-induced cells. To determine if fewer outer doublets were present at either the distal end of the flagellum or the proximal end, we quantified the number of outer doublets present at various positions along the axoneme (Fig. 5). As the flagellum of *T. brucei* is attached to the cell body, which has different widths and morphology along its length, it is possible to position an axonemal profile in any given electron micrograph to a particular region of the

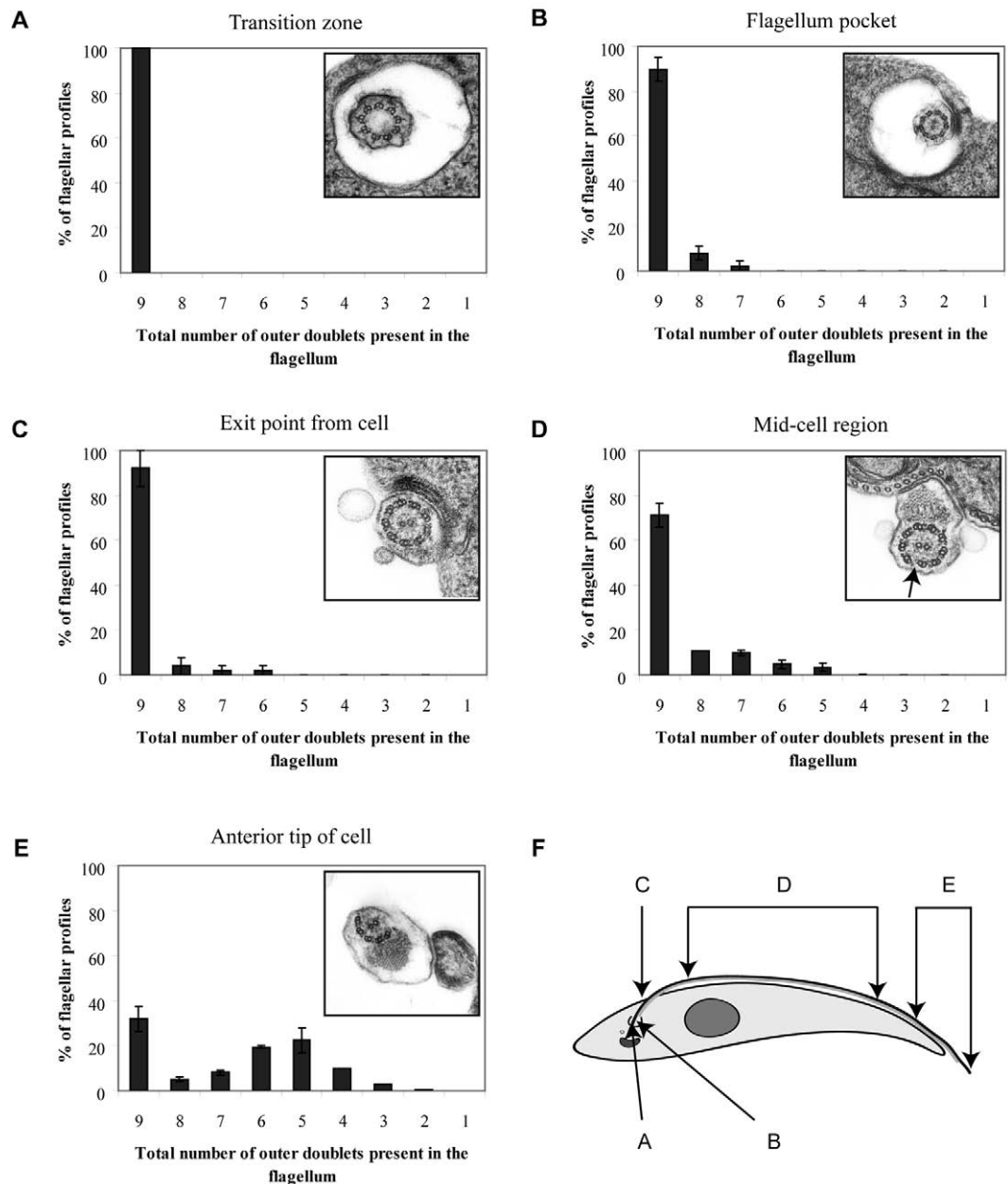


**Fig. 5.** Multiple outer-doublet loss occurs more frequently at the anterior of the cell. (A-E) The number of outer doublets was quantified at various positions along the axoneme. Graphs show the number of outer doublets present plotted against the frequency of occurrence in flagella profiles observed. Inset images show representative micrographs of flagella profiles at each position. The arrow in D indicates the break between two outer doublets that is observed prior to doublet loss. (F) Drawing of a *T. brucei* cell indicating the positions along the flagellum quantified in A-E.

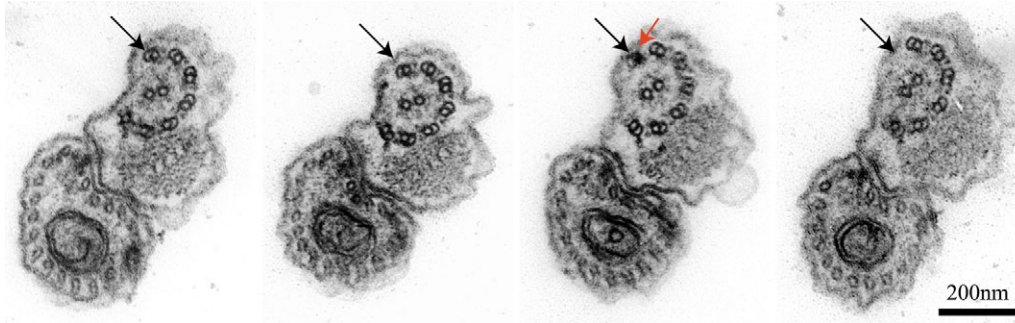


**Fig. 6.** The A and B tubules terminate simultaneously. Serial electron micrographs (left to right) showing loss of an outer doublet along a single axoneme. The black arrows indicate the position of the doublet that will be lost. Note the electron-dense lumen in the A tubule (red arrow) immediately prior to doublet loss. Bar, 200 nm.

flagellum. We characterised flagellar profiles into five subsets according to the adjacent cellular structures: transition zone, flagellum pocket, exit point of flagellum from cell, mid-cell region and anterior tip of cell. The basal bodies (data not shown) and transition zones (Fig. 5A) of RNAi-induced flagella appeared normal. Over 90% of axonemes found within, or just exiting the flagellar pocket had nine outer doublets, with only a minority having up to three doublets missing (Fig. 5B,C, respectively). However, the number of outer doublets decreased significantly from then on along the length of the cell body (Fig. 5D), such that at the distal tip of the flagellum only 32% of axonemes exhibited a 9+2 configuration, with 55% composed of six or fewer outer doublets (Fig. 5E).

We next examined serial thin-section micrographs to establish whether the missing doublets resulted from doublet termination. We focussed on the region close to the distal tip of the flagellum, where little or no cell body was visible, as this was where most doublets appeared to be lost (Fig. 5E). Serial sectioning through the distal tip region revealed that both the A and B tubules of a doublet terminated simultaneously (Fig. 6, black arrows show the doublet that is lost). An electron-dense lumen was observed only in the A tubule (Fig. 6, red arrow) immediately prior to the loss of that doublet, similar to that observed in capped *Chlamydomonas* flagella (Dentler, 1980), suggesting that the doublet may be capped prior to termination.

#### GFP-TbPACRG fusion proteins localise to the axoneme

To localise each of the two TbPACRG proteins within *T. brucei*, one copy of the two endogenous genes (*T. brucei* is diploid) was replaced with a GFP-TbPACRG fusion. Strains were constructed individually expressing GFP-TbPACRG A or GFP-TbPACRG B. In both instances, live cells exhibited a fluorescent flagellum. We performed immunofluorescence on detergent-extracted cytoskeletons using anti-GFP polyclonal antibody (Invitrogen) and antibodies against the paraflagellar rod (L8C4) (Kohl et al., 1999) or against the distal end of the basal body (BBA4) (Woods et al., 1989). The anti-GFP staining ran along the entire length of the flagellum in cells expressing either TbPACRG A, (Fig. 7A,B) or TbPACRG B (Fig. 7C,D). We investigated to which subcompartment of the flagellum TbPACRG A was localised using dual labelling with antibodies to both the basal body and the PFR. The anti-GFP signal (Fig. 7F, green, arrow) extended beyond that of the PFR (Fig. 7F, red), suggesting that GFP-PACRG is localised to the axoneme and not the PFR. No staining was apparent in the

basal body (Fig. 7H, red staining marks the distal end of the basal body), suggesting that TbPACRG appears in the flagellum distal to this structure. These localisation experiments were performed independently for both TbPACRG A and TbPACRG B, with identical results.

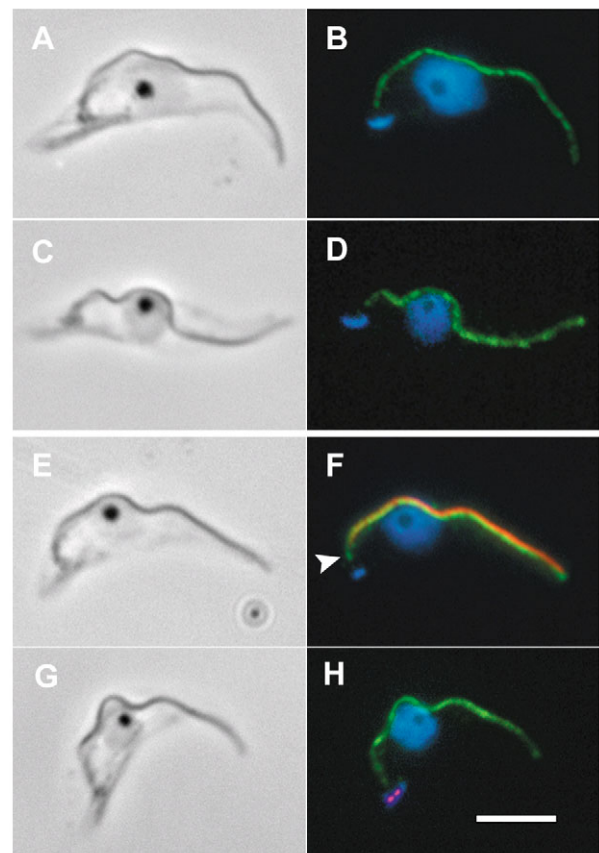


**Fig. 7.** GFP-TbPACRG fusion proteins localise to the axoneme. Phase-contrast microscopy (A,C,E,G) and fluorescence (B,D,F,H) images of detergent-extracted trypanosome cytoskeletons. DNA is labelled with DAPI (blue), and GFP is identified by anti-GFP polyclonal antibody (green). (A,B) Cells expressing GFP-TbPACRG A. (C,D) Cells expressing GFP-TbPACRG B. (E,F) Cells expressing GFP-TbPACRG A where the PFR is identified by the L8C4, anti-PFR, monoclonal antibody (red). Note the GFP signal extends proximal to the PFR staining (F, arrow). (G,H) Cells expressing GFP-TbPACRG A where the distal end of the basal body is identified by the BBA4 monoclonal antibody (red). Bar, 5 µm.

## Discussion

Our aim in this work was to characterise the location and function of the evolutionarily conserved protein PACRG. We have shown that TbPACRG A and TbPACRG B localise to the axoneme of the eukaryotic flagellum and that simultaneous ablation of TbPACRG A and B expression produces a dramatic motility phenotype caused by loss of outer-doublet microtubules. Taken together, our results identify a novel axonemal protein that we suggest plays a role in outer-doublet microtubule stability.

We have shown using bioinformatics that *T. brucei* possesses two closely related PACRG paralogues. Both are equally similar to mammalian PACRG and are most conserved in the C-terminal region. Two other kinetoplastid protozoa, *T. cruzi* and *L. major*, also possess two PACRG paralogues, indicating the situation in *T. brucei* is not the result of a recent gene duplication. To date we have no evidence to suggest functional differences between the two proteins. Although very similar at the protein level and therefore likely to have the same function, they are different enough at the nucleic acid level for us to select between them with RNAi. We find no obvious evidence of PACRG splice variants in the mammalian EST databases (data not shown); this cannot therefore explain the expansion of PACRG genes in kinetoplastids. Our data point to functional redundancy within the PACRG family in these organisms.

RNAi of TbPACRG A and B produces a major motility phenotype. Despite the lack of cell locomotion, the flagellum is built and at the light microscope level extends to essentially the same length as that observed in non-induced controls. There are, in addition, detectable cellular consequences for cell morphogenesis. First, the adversely affected new flagellum is associated with a mispositioning and/or malsegregation of the replicated mitochondrial genome, the kinetoplast. Kinetoplast position and segregation is known to be dependent upon basal body/flagellum connections and integrity (Ogbadoyi et al., 2003; Ploubidou et al., 1999; Robinson and Gull, 1991; Robinson et al., 1995). The kinetoplast mispositioning effect is likely to result from flagellum positioning/motility defects deriving from the absence of a full axoneme structure. The absence of this prevents effective function of motility and interaction with the connector that interlinks the tip of the new flagellum and the lateral aspect of the old. We have previously shown the importance of the flagella connector in trypanosome procyclic cell morphogenesis, and hypothesised that force applied by the new flagellum via connector attachment to the old is responsible for kinetoplast segregation in procyclic trypanosomes (Briggs et al., 2004; Moreira-Leite et al., 2001). Our present evidence shows that impairment of motility and flagellar connector action produces an ineffective movement of the new basal body/kinetoplast. Ultimately, such defects in cellular morphogenesis appear to accumulate and become compounded such that cell growth is affected.

A previous study has shown that mouse Pacrg was present in the sperm flagellum (Lorenzetti et al., 2004) but its localisation to a flagellar compartment or function was not elucidated. We used GFP-PACRG fusion proteins to confirm this general localisation in trypanosome flagella. We then examined to which subcompartment of the flagellum TbPACRG A and TbPACRG B localised. Our results show that both TbPACRG A and B localise along the full length of the axoneme but not to the basal body or PFR. Furthermore,

TbPACRG A and B are both present in a preparation of the detergent-insoluble flagellar fraction (our unpublished proteomic observations). One other protein is known to cause immotile sperm because of outer-doublet loss (Sampson et al., 2001). However, this protein, a voltage-dependent anion channel called VDAC3, localises to the outer dense fibres of sperm (Hinsch et al., 2004) rather than the axoneme and loss of only a single outer-doublet microtubule has been observed (Sampson et al., 2001). The presence of TbPACRG A and TbPACRG B along the whole length of the axoneme suggests that they are not required for outer-doublet initiation. Further evidence for this comes from the apparent absence of TbPACRG A and B from the basal body and transition zone regions, which appear normal by electron microscopy in TbPACRG AB RNAi-induced cells.

It is known that flagellar paralysis can result from loss of structures such as the PFR (Bastin et al., 1998), axonemal radial spokes and central pair (McKean et al., 2003; Smith and Lefebvre, 1997; Warr et al., 1966; Witman et al., 1978), however all these structures are present in TbPACRG AB RNAi-induced cells. The central pair remains present until more than four outer doublets have been lost, suggesting that this is a secondary effect of loss of multiple outer doublets. The presence of a PACRG homologue in the *C. elegans* genome, and EST evidence from mouse and human tissues containing primary (9+0) cilia (data not shown) support the idea that TbPACRG A and B are involved in the formation of outer-doublet microtubules but not the central pair.

In the majority of dividing cells, both the old and new flagella exhibited outer-doublet loss. This suggests that an affected old axoneme does not immediately stop morphogenesis of new axonemal/cytoskeletal architecture. This finding also demonstrates that the new axoneme starts to show doublet abnormalities before cytokinesis has occurred, during its late morphogenesis.

We tested whether there was variation in outer-doublet number along the length of an individual flagellum and found that it was normal at the proximal end of the flagellum and varied at the distal end, suggesting that axoneme formation is initiated normally. We do not yet know whether the outer-doublet microtubules grow to full length or are terminated prematurely. One possibility for PACRG function could be a role in outer-doublet extension. Depletion of PACRG would therefore lead to premature termination of outer-doublet microtubules, an idea supported by the capped A tubule seen in Fig. 6 prior to disappearance of that doublet. This explanation would fit with the observed increase in the number of missing microtubules along the flagellum, as observed in Fig. 5. The lack of random doublet termination around the axoneme would be explained by the fact that those doublets attached to the PFR would be preferentially stabilised by this connection. Alternatively, the microtubule outer doublets might be extended to their full length and then undergo partial catastrophe. Again, firmer linkages between doublets adjacent to the PFR could lead to their preferential stabilisation.

We have been unsuccessful at localising TbPACRG A or TbPACRG B at the ultrastructural level; nevertheless, aspects of the phenotype suggest possibilities for its sub-axonemal localisation. A likely candidate for its localisation would be the nexin interdoublet links (Fig. 4B). The interdoublet or nexin linkages have long been defined (Gibbons, 1965; Olson and

Linck, 1977; Stephens, 1970; Stephens and Edds, 1976; Warner, 1976) as an electron-dense band connecting the A tubule of one doublet to the B tubule of the adjacent doublet. It is proposed that these are elastic structures (Minoura et al., 1999) that enable the sliding of the doublets, yet their molecular identity remains unknown. It has been proposed that nexin links are in fact the dynein regulatory complex (DRC) (Woolley, 1997), a complex of six polypeptides (Huang et al., 1982; Piperno et al., 1992) of which only one has been characterised (Rupp and Porter, 2003). It is therefore possible that PACRG is a novel part of the DRC. A second study has localised the DRC to the junction between the radial spokes and the inner dynein arms (Gardner et al., 1994).

Various aspects of the TbPACRG AB RNAi phenotype support these ideas. Weakening of the nexin or other intermicrotubule linkages would be expected to lead to flagellar paralysis as the dynein-mediated interdoubtlet sliding that results in motility would be compromised. Premature termination of doublets could occur as a result of these weakened interdoubtlet linkages. We have observed axonemes containing nine outer-doublet microtubules where there is an apparent break in the connection between two adjacent doublets (e.g. inset in Fig. 5D, arrow indicates break), suggesting the integrity of the linkages may be compromised. One feature of the phenotype was the preferential loss of specific outer doublets. Those furthest from the PFR (9, 1 and 2) were most frequently lost, suggesting that the PFR may play a stabilising role. The physical connection between the PFR and doublets 4 and 7 is expected to reduce strain on the ring structure in this region by restricting lateral movement of the associated doublets, and hence stabilise the axoneme at this point. Further stabilisation here is likely to come from the linkage between doublets 5 and 6, which previous studies in other systems suggest are more stable than other interdoubtlet linkages (reviewed by Lindemann and Kanous, 1997). Loss of the intact ring structure of the axoneme would be expected to promote further loss of adjacent doublets owing to increased strain on the doublets located either side of the gap.

Although PACRG is predominantly expressed in the testis (Lorenzetti et al., 2004), EST evidence suggests a wider tissue distribution. Owing to the co-regulation of *PACRG* and *Parkin* in mammals, one study examined the role of PACRG in neurodegenerative disorders (Imai et al., 2003). In neuronal tissue, PACRG is found in neurodegenerative inclusions, where it is thought to form part of a complex that includes members of the chaperonin and heat shock protein (HSP) families including HSP70, HSP90 and various TCP1 members (Imai et al., 2003). It remains to be seen if PACRG has similar binding partners in the axoneme, but it is worth noting that cilia and flagella are known to contain an HSP70 family member (Bloch and Johnson, 1995; Stephens, 1997; Stephens and Lemieux, 1999; Williams and Nelsen, 1997), an HSP90 family member (Stephens and Lemieux, 1999; Williams and Nelsen, 1997) and a chaperonin of the TCP1 family (Cyrne et al., 1996; Soares et al., 1994; Stephens and Lemieux, 1999). In addition, an HSP40 family member has recently been identified as a component of the radial spoke complex (Satouh et al., 2005; Yang et al., 2005).

The repertoire of putative flagellar proteins of unknown function has recently been expanded by the application of comparative genomics and proteomics technologies. Our work

identifies PACRG as a novel and evolutionarily conserved axonemal component that plays a role in axonemal stability. The evolutionary conservation of PACRG highlights its importance in the axoneme and suggests it plays a fundamental role in axoneme stability in many eukaryotic organisms and cell types exhibiting both motile and sensory flagella. Although we have demonstrated its importance in motility in this work, we predict that PACRG is also necessary for the functioning of primary cilia. A challenge for the future will be to firmly identify the axonemal compartment where PACRG is located and to elucidate the molecular mechanisms that underlie its function.

We are grateful to Laura Briggs for early bioinformatic analyses and Steven Kelly for assistance with GFP tagging. We would also like to thank Dick McIntosh and members of the Gull lab for helpful discussions. This work was supported by the BBSRC and Wellcome Trust and a BBSRC studentship (H.F.). K.G. is a Wellcome Trust Principal Research Fellow.

## References

- Altschul, S. F., Madden, T. L., Schäffer, A. A., Zhang, J., Zhang, Z., Miller, W. and Lipman, D. J. (1997). Gapped BLAST and PSI-BLAST: a new generation of protein database search programs. *Nucleic Acids Res.* **25**, 3389-3402.
- Avidor-Reiss, T., Maer, A. M., Koundakjian, E., Polyanovsky, A., Keil, T., Subramaniam, S. and Zuker, C. S. (2004). Decoding cilia function: defining specialized genes required for compartmentalized cilia biogenesis. *Cell* **117**, 527-539.
- Bastin, P., Sherwin, T. and Gull, K. (1998). Paraflagellar rod is vital for trypanosome motility. *Nature* **391**, 548.
- Bloch, M. A. and Johnson, K. A. (1995). Identification of a molecular chaperone in the eukaryotic flagellum and its localization to the site of microtubule assembly. *J. Cell Sci.* **108**, 3541-3545.
- Briggs, L. J., McKean, P. G., Baines, A., Moreira-Leite, F., Davidge, J., Vaughan, S. and Gull, K. (2004). The flagella connector of *Trypanosoma brucei*: an unusual mobile transmembrane junction. *J. Cell Sci.* **117**, 1641-1651.
- Brun, R. and Schonenberger, M. (1979). Cultivation and in vitro cloning or procyclic culture forms of *Trypanosoma brucei* in a semi-defined medium. *Acta Trop.* **36**, 289-292.
- Cyrne, L., Guerreiro, P., Cardoso, A. C., Rodrigues-Pousada, C. and Soares, H. (1996). The Tetrahymena chaperonin subunit CCT eta gene is coexpressed with CCT gamma gene during cilia biogenesis and cell sexual reproduction. *FEBS Lett.* **383**, 277-283.
- Dentler, W. L. (1980). Structures linking the tips of ciliary and flagellar microtubules to the membrane. *J. Cell Sci.* **42**, 207-220.
- El Zein, L., Omran, H. and Bouvagnet, P. (2003). Lateralization defects and ciliary dyskinesia: lessons from algae. *Trends Genet.* **19**, 162-167.
- Gadella, C., Wickstead, B., de Souza, W., Gull, K. and Cunha-e-Silva, N. (2005). Cryptic paraflagellar rod in endosymbiont-containing kinetoplastid protozoa. *Eukaryot. Cell* **4**, 516-525.
- Gardner, L. C., O'Toole, E., Perrone, C. A., Giddings, T. and Porter, M. E. (1994). Components of a "dynein regulatory complex" are located at the junction between the radial spokes and the dynein arms in *Chlamydomonas* flagella. *J. Cell Biol.* **127**, 1311-1325.
- Gibbons, I. R. (1965). Chemical dissection of cilia. *Arch. Biol. (Liege)* **76**, 317-352.
- Gull, K. (1999). The cytoskeleton of trypanosomatid parasites. *Annu. Rev. Microbiol.* **53**, 629-655.
- Hinsch, K. D., De Pinto, V., Aires, V. A., Schneider, X., Messina, A. and Hinsch, E. (2004). Voltage-dependent anion-selective channels VDAC2 and VDAC3 are abundant proteins in bovine outer dense fibers, a cytoskeletal component of the sperm flagellum. *J. Biol. Chem.* **279**, 15281-15288.
- Huang, B., Ramanis, Z. and Luck, D. J. (1982). Suppressor mutations in *Chlamydomonas* reveal a regulatory mechanism for flagellar function. *Cell* **28**, 115-124.
- Imai, Y., Soda, M., Murakami, T., Shoji, M., Abe, K. and Takahashi, R.

- (2003). A product of the human gene adjacent to parkin is a component of Lewy bodies and suppresses Pael receptor-induced cell death. *J. Biol. Chem.* **278**, 51901-51910.
- Kohl, L., Sherwin, T. and Gull, K.** (1999). Assembly of the paraflagellar rod and the flagellum attachment zone complex during the *Trypanosoma brucei* cell cycle. *J. Eukaryot. Microbiol.* **46**, 105-109.
- Li, J. B., Gerdes, J. M., Haycraft, C. J., Fan, Y., Teslovich, T. M., May-Simera, H., Li, H., Blacque, O. E., Li, L., Leitch, C. C. et al.** (2004). Comparative genomics identifies a flagellar and basal body proteome that includes the BBS5 human disease gene. *Cell* **117**, 541-552.
- Lindemann, C. B. and Kanous, K. S.** (1997). A model for flagellar motility. *Int. Rev. Cytol.* **173**, 1-72.
- Lockhart, P. J., O'Farrell, C. A. and Farrer, M. J.** (2004). It's a double knock-out! The quaking mouse is a spontaneous deletion of parkin and parkin co-regulated gene (PACRG). *Mov. Disord.* **19**, 101-104.
- Lorenzetti, D., Bishop, C. E. and Justice, M. J.** (2004). Deletion of the Parkin coregulated gene causes male sterility in the quaking(viable) mouse mutant. *Proc. Natl. Acad. Sci. USA* **101**, 8402-8407.
- McKean, P. G., Baines, A., Vaughan, S. and Gull, K.** (2003). Gamma-tubulin functions in the nucleation of a discrete subset of microtubules in the eukaryotic flagellum. *Curr. Biol.* **13**, 598-602.
- Minoura, I., Yagi, T. and Kamiya, R.** (1999). Direct measurement of inter-doublet elasticity in flagellar axonemes. *Cell Struct. Funct.* **24**, 27-33.
- Moreira-Leite, F. F., Sherwin, T., Kohl, L. and Gull, K.** (2001). A trypanosome structure involved in transmitting cytoplasmic information during cell division. *Science* **294**, 610-612.
- Ogbadoyi, E. O., Robinson, D. R. and Gull, K.** (2003). A high-order transmembrane structural linkage is responsible for mitochondrial genome positioning and segregation by flagellar basal bodies in trypanosomes. *Mol. Biol. Cell* **14**, 1769-1779.
- Olson, G. E. and Linck, R. W.** (1977). Observations of the structural components of flagellar axonemes and central pair microtubules from rat sperm. *J. Ultrastruct. Res.* **61**, 21-43.
- Ostrowski, L. E., Blackburn, K., Radde, K. M., Moyer, M. B., Schlatter, D. M., Moseley, A. and Boucher, R. C.** (2002). A proteomic analysis of human cilia: identification of novel components. *Mol. Cell Proteomics* **1**, 451-465.
- Piperno, G., Mead, K. and Shestak, W.** (1992). The inner dynein arms I2 interact with a "dynein regulatory complex" in *Chlamydomonas* flagella. *J. Cell Biol.* **118**, 1455-1463.
- Ploubidou, A., Robinson, D. R., Docherty, R. C., Ogbadoyi, E. O. and Gull, K.** (1999). Evidence for novel cell cycle checkpoints in trypanosomes: kinetoplast segregation and cytokinesis in the absence of mitosis. *J. Cell Sci.* **112**, 4641-4650.
- Robinson, D. R. and Gull, K.** (1991). Basal body movements as a mechanism for mitochondrial genome segregation in the trypanosome cell cycle. *Nature* **352**, 731-733.
- Robinson, D. R., Sherwin, T., Ploubidou, A., Byard, E. H. and Gull, K.** (1995). Microtubule polarity and dynamics in the control of organelle positioning, segregation, and cytokinesis in the trypanosome cell cycle. *J. Cell Biol.* **128**, 1163-1172.
- Rupp, G. and Porter, M. E.** (2003). A subunit of the dynein regulatory complex in *Chlamydomonas* is a homologue of a growth arrest-specific gene product. *J. Cell Biol.* **162**, 47-57.
- Sampson, M. J., Decker, W. K., Beaudet, A. L., Ruitenbeek, W., Armstrong, D., Hicks, M. J. and Craigen, W. J.** (2001). Immotile sperm and infertility in mice lacking mitochondrial voltage-dependent anion channel type 3. *J. Biol. Chem.* **276**, 39206-39212.
- Satouh, Y., Padma, P., Toda, T., Satoh, N., Ide, H. and Inaba, K.** (2005). Molecular characterization of radial spoke subcomplex containing radial spoke protein 3 and heat shock protein 40 in sperm flagella of the ascidian *Ciona intestinalis*. *Mol. Biol. Cell* **16**, 626-636.
- Sherwin, T. and Gull, K.** (1989). The cell division cycle of *Trypanosoma brucei*: timing of event markers and cytoskeletal modulations. *Philos. Trans. R. Soc. London B Biol. Sci.* **323**, 573-588.
- Sidman, R. L., Dickie, M. M. and Appel, S. H.** (1964). Mutant mice (quaking and jimpy) with deficient myelination in the central nervous system. *Science* **144**, 309-311.
- Smith, E. F. and Lefebvre, P. A.** (1997). The role of central apparatus components in flagellar motility and microtubule assembly. *Cell Motil. Cytoskeleton* **38**, 1-8.
- Soares, H., Penque, D., Mouta, C. and Rodrigues-Pousada, C.** (1994). A *Tetrahymena* orthologue of the mouse chaperonin subunit CCT gamma and its coexpression with tubulin during cilia recovery. *J. Biol. Chem.* **269**, 29299-29307.
- Stephens, R. E.** (1970). Isolation of Nexin - The linkage protein responsible for the maintenance of the nine-fold configuration of flagellar axonemes. *Biol. Bull.* **139**, 438.
- Stephens, R. E.** (1997). Synthesis and turnover of embryonic sea urchin ciliary proteins during selective inhibition of tubulin synthesis and assembly. *Mol. Biol. Cell* **8**, 2187-2198.
- Stephens, R. E. and Edds, K. T.** (1976). Microtubules: structure, chemistry, and function. *Physiol. Rev.* **56**, 709-777.
- Stephens, R. E. and Lemieux, N. A.** (1999). Molecular chaperones in cilia and flagella: implications for protein turnover. *Cell Motil. Cytoskeleton* **44**, 274-283.
- Thompson, J. D., Gibson, T. J., Plewniak, F., Jeanmougin, F. and Higgins, D. G.** (1997). The CLUSTAL X windows interface: flexible strategies for multiple sequence alignment aided by quality analysis tools. *Nucleic Acids Res.* **25**, 4876-4882.
- Warner, F. D.** (1976). Ciliary inter-microtubule bridges. *J. Cell Sci.* **20**, 101-114.
- Warr, J. R., McVitte, A., Randall, J. and Hopkins, J. M.** (1966). Genetic control of flagellar structure in *Chlamydomonas reinhardtii*. *Genet. Res.* **7**, 335-351.
- West, A. B., Lockhart, P. J., O'Farrell, C. and Farrer, M. J.** (2003). Identification of a novel gene linked to parkin via a bi-directional promoter. *J. Mol. Biol.* **326**, 11-19.
- Wickstead, B., Ersfeld, K. and Gull, K.** (2002). Targeting of a tetracycline-inducible expression system to the transcriptionally silent minichromosomes of *Trypanosoma brucei*. *Mol. Biochem. Parasitol.* **125**, 211-216.
- Williams, N. E. and Nelsen, E. M.** (1997). HSP70 and HSP90 homologs are associated with tubulin in hetero-oligomeric complexes, cilia and the cortex of *Tetrahymena*. *J. Cell Sci.* **110**, 1665-1672.
- Wirtz, E., Leal, S., Ochatt, C. and Cross, G. A.** (1999). A tightly regulated inducible expression system for conditional gene knock-outs and dominant-negative genetics in *Trypanosoma brucei*. *Mol. Biochem. Parasitol.* **99**, 89-101.
- Witman, G. B., Plummer, J. and Sander, G.** (1978). *Chlamydomonas* flagellar mutants lacking radial spokes and central tubules. Structure, composition, and function of specific axonemal components. *J. Cell Biol.* **76**, 729-747.
- Woods, A., Sherwin, T., Sasse, R., MacRae, T. H., Baines, A. J. and Gull, K.** (1989). Definition of individual components within the cytoskeleton of *Trypanosoma brucei* by a library of monoclonal antibodies. *J. Cell Sci.* **93**, 491-500.
- Woolley, D. M.** (1997). Studies on the eel sperm flagellum. I. The structure of the inner dynein arm complex. *J. Cell Sci.* **110**, 85-94.
- Yang, C., Compton, M. M. and Yang, P.** (2005). Dimeric novel HSP40 is incorporated into the radial spoke complex during the assembly process in flagella. *Mol. Biol. Cell* **16**, 637-648.